Received 5 December 2006
Revised 25 May 2007
Accepted 25 May 2007

Verification of a numerical model of macrosegregation in direct chill casting

Miha Založnik
Impol Aluminium Industry, Slovenska Bistrica, Slovenia and Laboratoire de Science et Génie des Matériaux Métalliques, Ecole des Mines de Nancy, Nancy, France

Shihe Xin
LIMSI-CNRS, Orsay, France and CETHIL, Villeurbanne, France, and

Božidar Šarler
Laboratory for Multiphase Processes, University of Nova Gorica, Nova Gorica, Slovenia

Abstract

Purpose – This paper aims to point out the critical problems in numerical verification of solidification simulation codes and the complexity of the verification and to propose and apply a procedure of generalized verification for macrosegregation simulation.

Design/methodology/approach – A partial verification of a finite-volume computational model of macrosegregation in direct chill (DC) casting of binary aluminum alloys, including the coupled transport phenomena of heat transfer, fluid flow and species transport, is performed. The verification procedure is conducted on numerical test problems, defined as subproblems with respect to the complexity of the physical model, geometry, and boundary conditions. The studied cases are thermal convection with solidification in DC casting, thermal natural convection of a low-Prandtl-number liquid metal in a rectangular cavity and 1D directional solidification of a binary Al-Cu alloy. Grid-convergence studies, code comparison with an alternative Chebyshev-collocation method, and comparison with a reference similarity solution are used for verification.

Findings – An excellent ability of the model to accurately resolve the thermal convection in the pertinent range of Prandtl and Rayleigh numbers is shown. Concerns regarding the solution of species transport in the mushy zone remain.

Research limitations/implications – The proposed verification procedure is not completed in its entirety. Further verification of the solutal and thermosolutal convection problems is required.

Originality/value – This paper proposes verification techniques for complex coupled solidification problems involving significant convection in the melt.

Keywords Solidification, Convection, Flow, Modeling

Paper type Research paper

1. Introduction

Direct chill (DC) casting is one of the most widely used industrial light metal processing technologies. Macrosegregation, an inhomogeneous distribution of alloying elements at

The first author would like to thank Dr Dominique Gobin for many helpful discussions and suggestions.

International Journal of Numerical Methods for Heat & Fluid Flow
Vol. 18 No. 3/4, 2008
pp. 308-324

0961-5539
DOI 10.1108/09615530810853600

the scale of the solidified casting, is a common defect that occurs in DC casting of aluminum alloys. It is a direct consequence of the transport phenomena taking place during the solidification process. It is caused by advective solute transport primarily due to the flow of segregated liquid in the mushy solidification zone. This laminar flow is a result of convection in the liquid part, driven by buoyancy forces due to thermal gradients (thermal natural convection), buoyancy forces due to concentration gradients (solutal natural convection), and inlet flow (bulk convection). Additionally, a feeding flow due to density differences between the two phases (solidification shrinkage) is induced in the mushy zone. The coupled transport of heat, species and momentum is characterized by low-Prandtl numbers ($Pr \sim 10^{-2}$), high-Schmidt numbers ($Sc \sim 10^{2}$), and high-thermal and solutal Rayleigh numbers ($Ra_{T} \sim 10^{6}, \ldots 10^{7}$, $Ra_{C} \sim 10^{11}$). Macrosegregation can lead to nonuniform mechanical properties, which affect the behavior of the metal during subsequent treatments and impair the quality of the final product. It is therefore desirable to be able to simulate the casting process in order to predict the influence of casting parameters on the resulting macrosegregation pattern. Besides, the prediction, modeling is aimed at improving understanding of the basic mechanisms involved.

Recent numerical results (Založnik and Šarler, 2005a) led to the hypothesis that the DC casting parameters affect macrosegregation through their direct effect on the structure of the thermosolutal natural convection flow – the driving flow in the liquid part of the solidifying casting. In view of the final objective of development of a predictive model, this finding motivates a more rigorous verification procedure and the determination of requirements for numerical accuracy in the modeling of the predominantly advective transport of momentum and species as is the case during solidification of metal alloys. A further incentive for verification is the fact that previously presented models of macrosegregation in DC casting (Reddy and Beckermann, 1997; Vreeman and Incropera, 2000; Jalanti *et al.*, 2001) did not demonstrate a rigorous verification procedure and that no clear numerical reference results for the casting problem exist. The efforts to clarify some of the numerical issues were recently made by Venneker and Katgerman (2002).

The present paper details a partial verification of a finite-volume numerical model developed for macrosegregation in DC casting. Numerical results obtained in the simulations of DC casting of a binary aluminum alloy (Al-5.25%Cu) show a complex multicellular thermosolutal flow structure. The aforementioned hypothesis on the effect of casting parameters (Založnik and Šarler, 2005a), particularly in view of the complex coupling of the transport of heat, momentum, and species and the difficult numerical modeling of predominantly advective transport, indicates the need for a stepwise verification of the simulation code on smaller "subproblems." The verification is thus conducted with three subproblems of the DC casting problem. The first two aim to check the accuracy of the numerical solution of the flow field and the thermal natural convection problem. The third one verifies the coupling between the macroscopic heat and species transport in the mushy zone and the microsegregation model. The verification results presented in this first phase are satisfactory and further verification steps are outlined.

2. Model description

2.1 Macroscale transport model

The one-phase continuum mixture model developed by Bennon and Incropera (1987) is used to describe the solidification system. The macroscopic conservation equations are

transport equations for heat, mass, momentum, and species, simultaneously valid in the liquid, mushy, and solid regions. A rigid and connected solid phase is assumed, forming a porous structure (mush) in the phase change zone. In the one-phase model the two-phase (solid-liquid) mixture is described using mass fractions (f_k) and volume fractions (g_k) of solid ($k = s$) and liquid ($k = \mathrm{l}$) phases, defined as follows:

$$f_k = \frac{m_k}{m_\mathrm{s} + m_\mathrm{l}} \quad g_k = \frac{V_k}{V_\mathrm{s} + V_\mathrm{l}} = \frac{\rho_\mathrm{m}}{\rho_k} f_k \tag{1}$$

$$f_\mathrm{s} + f_\mathrm{l} = 1, \tag{2}$$

where m is the mass and V is the volume of the respective phase and subscript "m" denotes the mixture. In the framework of a one-phase representation of the solid-liquid mixture, the mixture density ρ_m, velocity $\vec{v}_\mathrm{m}$, enthalpy h_m, and concentration C_m are defined:

$$\rho_\mathrm{m} = g_\mathrm{s}\rho_\mathrm{s} + g_\mathrm{l}\rho_\mathrm{l}, \quad \vec{v}_\mathrm{m} = f_\mathrm{s}\vec{v}_\mathrm{s} + f_\mathrm{l}\vec{v}_\mathrm{l}, \quad h_\mathrm{m} = f_\mathrm{s}h_\mathrm{s} + f_\mathrm{l}h_\mathrm{l}, \quad C_\mathrm{m} = f_\mathrm{s}C_\mathrm{s} + f_\mathrm{l}C_\mathrm{l}. \tag{3}$$

In the computations presented in this paper, two slightly different models are used. In the macrosegregation computations, the full thermal and solutal solidification model is used. In the verification cases for thermal convection, a simplified thermal solidification model, which disregards species transport, however retains a solidification interval and a mushy zone, is employed. The full model is described hereafter and the simplifications made in the thermal solidification model are noted on the way.

The governing equations are formulated in terms of the mixture quantities, for which they are solved. Nevertheless, it is inevitable that terms containing phase quantities are retained. They are expressed as correction "source" terms, appearing as last terms on the right hand side in the equations given below. The continuity equation for the mixture retains the form valid for one phase:

$$\frac{\partial \rho_\mathrm{m}}{\partial t} + \nabla \cdot (\rho_\mathrm{m}\vec{v}_\mathrm{m}) = 0. \tag{4}$$

The mixture momentum conservation equation is:

$$\begin{aligned} \frac{\partial \rho_\mathrm{m}\vec{v}_\mathrm{m}}{\partial t} + \nabla \cdot (\rho_\mathrm{m}\vec{v}_\mathrm{m}\vec{v}_\mathrm{m}) = &- \nabla p + \nabla \cdot \left(\mu_\mathrm{l} \frac{\rho_\mathrm{m}}{\rho_\mathrm{l}} \nabla \vec{v}_\mathrm{m} \right) - \frac{\mu_\mathrm{l}}{K} \frac{\rho_\mathrm{m}}{\rho_\mathrm{l}} (\vec{v}_\mathrm{m} - \vec{v}_\mathrm{s}) \\ &- \rho_0 \vec{g} [\beta_\mathrm{T}(T - T_0) + \beta_\mathrm{C}(C_\mathrm{l} - C_0)] - \nabla \cdot [\rho_\mathrm{m}(f_\mathrm{s}\vec{v}_\mathrm{s}\vec{v}_\mathrm{s} \\ &+ f_\mathrm{l}\vec{v}_\mathrm{l}\vec{v}_\mathrm{l} - \vec{v}_\mathrm{m}\vec{v}_\mathrm{m})], \end{aligned} \tag{5}$$

where p is the pressure, μ_l is the liquid viscosity, K is the permeability of the porous mush, ρ_0 is the reference density, $\vec{g}$ is the gravity acceleration, β_T and β_C are the thermal and solutal volumetric expansion coefficients, respectively, T is the temperature, and T_0 and C_0 are the reference temperature and concentration. The velocity of the solid is defined to be equal to the casting velocity ($\vec{v}_\mathrm{s} = \vec{v}_\mathrm{cast}$) everywhere, since all solid mush is assumed to be coalesced in a porous matrix and connected with the bulk solid. The permeability is modeled by the Kozeny-Carman relation $K = K_0 g_l^3/(1 - g_\mathrm{l})^2$. In the thermal solidification model the solutal buoyancy

term is zero, since the concentration is assumed to be homogeneous. The diffusive term in the energy conservation equation (Fourier law) is reformulated in terms of the mixture enthalpy using the following supplementary thermodynamic state equations:

$$h_s(T) = h_{ref} + \int_{T_{ref}}^{T} c_{ps}\mathrm{d}T \quad h_l(T) = h_s(T) + L_{eut} + \int_{T_{eut}}^{T} (c_{pl} - c_{ps})\mathrm{d}T, \tag{6}$$

where c_p is the specific heat, T_{eut} is the eutectic temperature and L_{eut} is the latent heat of solidification of the primary phase at the eutectic. The mixture energy conservation equation is thus written:

$$\begin{aligned}\frac{\partial(\rho_m h_m)}{\partial t} + \nabla\cdot(\rho_m \vec{v}_m h_m) = \nabla\cdot\left(\frac{k}{c_{ps}}\nabla h_m\right) + \nabla\cdot\left(\frac{k}{c_{ps}}\nabla(h_s - h_m)\right) \\ - \nabla\cdot[\rho_m(f_s\vec{v}_s h_s + f_l\vec{v}_l h_l - \vec{v}_m h_m)],\end{aligned} \tag{7}$$

where k is the thermal conductivity of the mixture. The mixture species conservation equation is:

$$\begin{aligned}\frac{\partial(\rho_m C_m)}{\partial t} + \nabla\cdot(\rho_m \vec{v}_m C_m) = \nabla\cdot(\rho_m D_m \nabla C_m) \\ + \nabla\cdot[\rho_m(f_s D_s \nabla C_s + f_l D_l \nabla C_l - D_m \nabla C_m)] \\ - \nabla\cdot[\rho_m(f_s\vec{v}_s C_s + f_l\vec{v}_l C_l - \vec{v}_m C_m)],\end{aligned} \tag{8}$$

where D is the molecular diffusivity. In the thermal solidification model the species conservation equation is omitted.

2.2 Microsegregation model

The phase quantities (f_s, f_l, $\vec{v}_s$, $\vec{v}_l$, h_s, h_l, C_s, C_l) and the temperature T, which still appear in the mixture transport equations, (4), (5), (7) and (8), are modeled in the following way. According to the aforementioned assumption, $\vec{v}_s = \vec{v}_{cast}$ and, consequently, equations (2) and (3) yield $\vec{v}_l = [\vec{v}_m - (1 - f_l)\vec{v}_{cast}]/f_l$. Further, the unknowns f_s, h_s, and h_l can be eliminated using equations (2) and (6). The solid concentration C_s is determined by the partitioning that follows from the inverse lever rule and an equilibrium solid-liquid partition ratio k_p:

$$C_s = k_p C_l. \tag{9}$$

The remaining three unknowns f_l, C_l, and T are determined by solving a system of three equations: the definition of mixture enthalpy (equation (10)), derived from equations (3) and (6), the inverse lever rule (equation (11)), which can be derived from equations (3) and (9), and an additional equation, describing the linearized liquidus line equation (12):

$$h_m(T, f_l) = \int_{T_{ref}}^{T} c_{ps}\mathrm{d}T + f_l\left[L_{eut} + \int_{T_{eut}}^{T} (c_{pl} - c_{ps})\mathrm{d}T\right], \tag{10}$$

$$C_l = \frac{C_m}{k_p + f_l(1 - k_p)}, \tag{11}$$

$$T(C_l) = T_f + m_L C_l, \tag{12}$$

where T_f is the melting temperature of the pure solvent and m_L is the slope of the liquidus line in the binary phase diagram. By substitution of variables in equations (10)–(11) a quadratic equation for f_l in the form $F(f_l) = 0$ is obtained, which is solved analytically for f_l. Then the temperature T is calculated from equation (10) and the liquid concentration C_l from equation (12). Further, the solid concentration C_s is calculated from equation (9), and the phase enthalpies h_s and h_l from their definitions in equation (6).

In the thermal solidification model, the concentrations C_s and C_l are not defined. The model is closed by using equation (10) and the assumption of a linear temperature dependence of f_l:

$$f_l = \frac{T - T_S}{T_L - T_S}, \tag{13}$$

where the solidus (T_S) and liquidus temperatures (T_L) are constant, at values corresponding to the nominal concentration.

2.3 Solution method

In the macrosegregation code the set of macroscopic transport equations (4), (5), (7) and (8) is solved with the finite volume method (FVM). The code supports Cartesian and axisymmetric geometries discretized by orthogonal grids. Dirichlet, Neumann or Robin type boundary conditions can be selected at individual boundaries, which enabled a straightforward use of a single numerical code in all verification cases presented in this paper. For the discretization of advective fluxes the second-order centered-difference scheme is used in the energy equation, giving effective and accurate solution. In the momentum and species conservation equations different schemes can be used. In the computation of macrosegregation in DC casting, the first-order upwind scheme is used in order to cure severe problems with iterative convergence of the coupled equation system, which are encountered when higher-order schemes are used for momentum advection. Note that this is only a preliminary computational framework that works efficiently. It is used before an efficient implementation of more accurate numerical schemes, which have been shown to be necessary to model the predominantly advective transport of species and momentum (Založnik and Šarler, 2005b), is completed. In all subsequently presented verification cases the third-order accurate QUICK scheme (Leonard, 1997) is used for both momentum and species. The SIMPLE algorithm (Ferziger and Perić 2002) is employed for pressure-velocity coupling and implicit Euler timestepping is used in the transient computations.

In the verification problem treating thermal natural convection in a cavity, the results of the macrosegregation code (FVM) are compared to those obtained by a spectral Chebyshev-collocation method (SCM). The spectral method is implemented in a numerical code tailored for the simulation of thermal natural convection in enclosures under the Boussinesq assumption. It employs either a projection method or the direct Uzawa method for pressure-velocity coupling and three-level semi-implicit second-order time stepping. A more detailed description of the code is given in Xin and Le Quéré (2002).

3. Macrosegregation in DC casting

The motivation for a subsequent more detailed verification of the developed macrosegregation code is given by the intricate flow predicted in simulations of DC casting. The results of a computation of macrosegregation in the DC casting of an Al-5.25%Cu alloy axisymmetric billet are shown in Figure 1. The computation was performed on an axisymmetric domain of 0.141 m radius and 0.6 m length (only the interesting top part is shown in all figures) assumed as adiabatic at the bottom boundary. A 100 × 356 control-volume (CV) grid was used. The grid was strongly biased in the top part ($z > -0.15$ m, the height of the liquid and mushy regions), such that this part was discretized into 100 × 200 equal CVs and the remaining bottom part into 100 × 156 CVs with a constant grid expansion factor of 1.0175. All physical parameters are specified in Tables AI and AII in the Appendix. Figure 1(a) shows the flow field together with the liquid-density field (calculated according to the Boussinesq approximation used in the momentum equation (5)). As can be seen in the plot, the liquid is relatively quiescent at the bottom and in the center of the liquid sump, which appears to be caused by the counteracting effect of thermal buoyancy and the layering tendency of the heavy solute-rich liquid. Next to the liquid-mush interface a complex flow structure, consisting of small vortices forms. Five vertically arranged flow cells can be identified, delimited by sharp density gradients. Each cell contains one or two vortices of thermosolutal origin. Such a multicellular structure occurs in thermosolutal flows, when a stable solutal stratification is destabilized by a large enough lateral temperature gradient (Gobin and Bennacer, 1996). The coupling of the thermal and solutal driving forces and the advective transport of heat and solute also causes a vertical density bump inside each thermosolutal cell and raises the splitting of the flow into two vortices. The flow structure close to the liquidus front appears to be very complex and more detailed studies seem to be necessary to determine and explain it more accurately. In the porous mushy zone (between the liquid-fraction isolines $f_l = 0$ and $f_l = 1$ in Figure 1) the dominant mechanism of solute transport is the flow driven by solidification shrinkage due to the higher density of the solid. It is directed perpendicular to the liquid-fraction gradient, as indicated in Figure 1(a).

4. Outline of the verification procedure

To be able to give a plausible sense to the flow structure observed in the DC casting simulation and construct a physical explanation of it, an accurate and verified numerical solution of the coupled problem is required. As there exist no reference solutions to the fully coupled problem, which would tremendously facilitate verification, it is difficult and unreasonable to consider the fully coupled problem as a test case and perform a numerical study of it. Because of the intricate coupling of the thermosolutal buoyancy driven flow, the heat and solute transport, solidification, and microsegregation in the mushy zone, i.e. complex physical phenomena involved, a stepwise verification procedure on subproblems is more feasible. Several subproblems – simplifications with respect to the complexity of the physical model, geometry, and boundary conditions – are proposed to test the solutions of individual transport equations and equation couplings in the pertinent parameter range, estimated as $Ra_T \sim 10^6, \ldots 10^7$, $Pr \sim 10^{-2}$, $Sc \sim 10^2$. The ability of the code to properly resolve the thermal-convection flow in the low-Pr liquid is assessed on the following two subproblems.

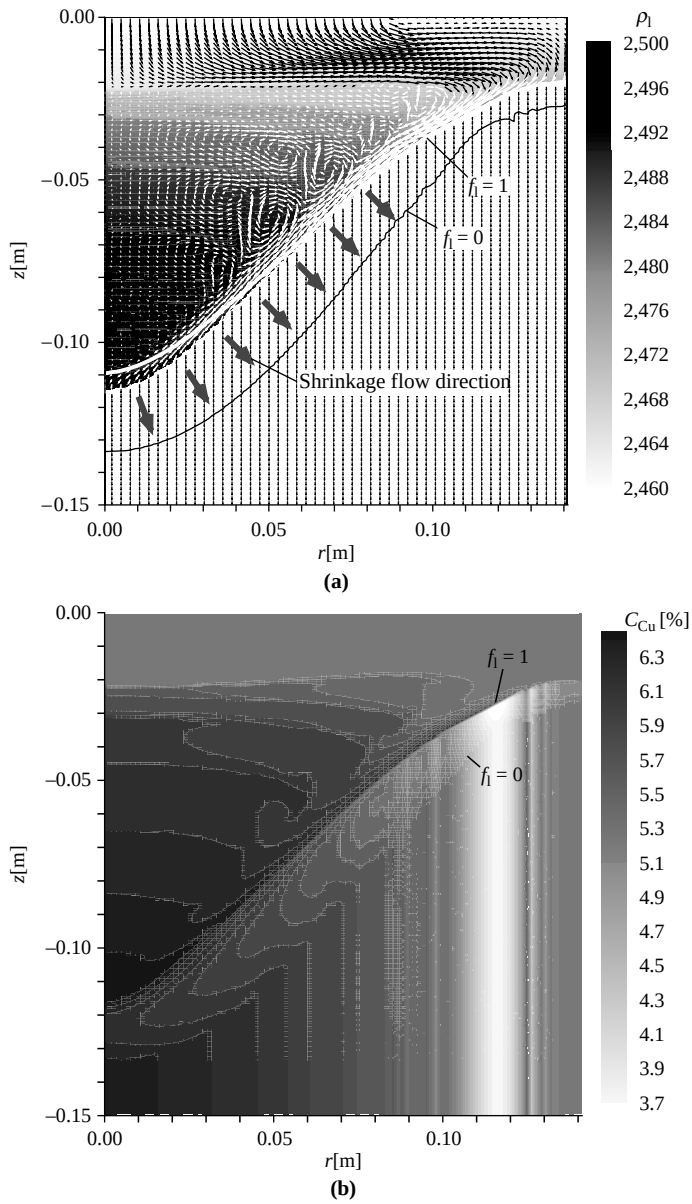

Notes: (a) Liquid density ($\rho_1 = \rho_0 [\beta_T (T - T_0) + \beta_C (C_1 - C_0)]$) and velocity ($\vec{v}_m$) fields in the axisymmertric billet obtained in the full macrosegregation computation. The density field is shown only in the liquid and part of the mushy zone ($f_1 > 0.9$); (b) Mixture Cu concentration (C_m) field in the billet

Figure 1.
Results of a computation of macrosegmentation

4.1 Thermal convection in DC casting

This problem retains the realistic geometry, boundary conditions, the coupling between the thermal and flow field, the interaction of the flow with the mushy zone and a simplified treatment of alloy solidification, while omitting the influence of the composition on the buoyancy force and on solidification. A reference solution does not exist. The numerical solution can be investigated by a grid convergence study. A confrontation with solutions obtained by an alternative code and numerical method (Perko, 2005) is planned later.

4.2 Thermal natural convection in a rectangular cavity

A numerically demanding prototypal problem for transient thermal buoyancy driven flow in metals on a simplified geometry, with simple boundary conditions and without solidification is studied. While a reference solution is presently not available, this problem enables verification by a detailed comparison to the solution, which was independently obtained with an extensively tested Chebyshev spectral code. The results of the presented comparison also present a starting point for the anticipated definition of a benchmark problem related to flow in metal solidification systems.

The coupling of the macroscopic heat and species transport and microsegregation is checked by a confrontation to a reference solution.

4.3 1D inverse macrosegregation in directional solidification

The numerical solution is compared to the semi-analytical similarity solution, developed by Voller (1997b), which transforms the governing partial differential equations into a set of ordinary differential equations. The similarity solution describes the macrosegregation induced by the 1D flow due to solidification shrinkage feeding in bottom-cooled directional solidification of a binary alloy. It includes a complete coupling of concentration and temperature fields in the mushy region, shrinkage fluid flow, and microsegregation with an eutectic reaction.

The aforementioned test cases represent a partial verification of the model. Further tests, aiming at the evaluation of the ability of the code to properly resolve the advective solute transport and the (low-*Pr*, high-*Sc*) thermosolutal flow are planned (Založnik, 2006). The first one is a test case for thermosolutal natural convection in a rectangular cavity for high *Pr* and high *Sc*. It focuses on the verification of the species transport. It features basic parameters of thermosolutal buoyancy-driven flow, as it omits instabilities inherent in low-*Pr* thermal convection. The results can be compared to solutions published by Gobin and Bennacer (1996). The second test case considers thermosolutal natural convection in a rectangular cavity for low *Pr* and high *Sc*, which represents the relevant parameter range for buoyancy-driven flow in metals. It means a much less stable parameter range, since the flow is characterized by regions where it is controlled by a balance of thermal and solutal buoyancy driving forces and inertia, and only weak influence of viscous forces.

5. Thermal convection in DC casting

The adequacy of the numerical model for the solution of the flow field is studied in more detail on the simplified thermal solidification model of DC casting, described in Section 2. Species transport is not taken into account, thus reducing the problem to one of coupled convective heat transfer and fluid flow. Apart from the solidus and liquidus

temperatures, which are fixed at values corresponding to the nominal composition of Al-5.25%Cu ($T_S = 827$ K, $T_L = 920$ K) all parameters are the same as in the previously presented macrosegregation computation. Also the biased computational grids are constructed by the same principles (uniformly meshed top part at $z > -0.15$ m and a coarsening grid with a constant grid expansion factor in the bottom part). Part of the results of a grid convergence study are shown in Figure 2, where streamlines in the axisymmetric billet in the final steady state are shown as obtained in calculations on four different computational grids. An evolution of the solution into a multicellular flow is observed with grid refinement, and an apparently grid independent solution is obtained with very fine grids.

A more detailed characterization of grid convergence is provided in Table I, showing the convergence of global velocity and streamfunction minima (maxima in absolute values), i.e. of the L_∞ norm of the respective quantities, as well as of the discretized L_1 norm of the kinetic energy:

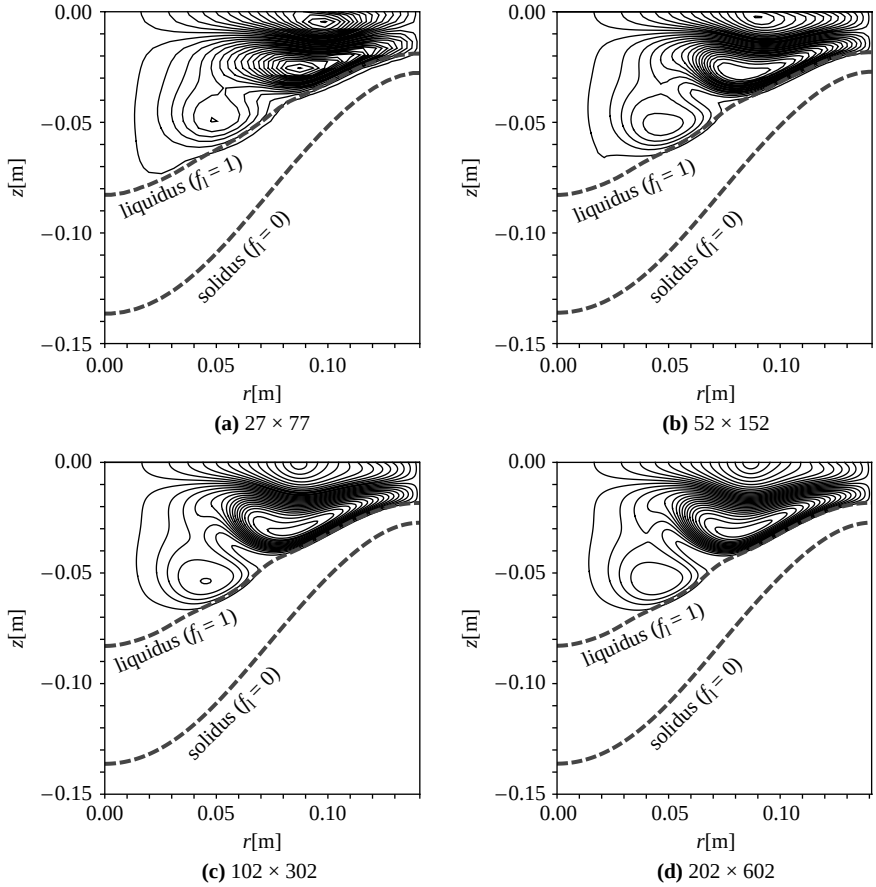

Note: Streamlines of relative velocity ($\vec{v} - \vec{v}_{cast}$) in the top part of the computational domain are shown as obtained on four finite-volume grids

Figure 2.
Grid convergence of the flow field in the axisymmetric billet for thermal convection in DC casting

$$\|E_k\|_1 = \frac{1}{2}\sum_i (f_{l,i}\rho_l + (1 - f_{l,i})\rho_s)(\Delta V)_i(u_i^2 + v_i^2). \quad (14)$$

Subscript i denotes the value at CV i and $(\Delta V)_i$ is the volume of the respective CV. An attempt to more clearly characterize grid convergence using Richardson extrapolation (Roy, 2005) was made by computing the observed order of convergence for the quantities in Table I over the three finer grids:

$$p_{\text{Rex}} = \frac{\ln(f_{52\times152} - f_{102\times302})/(f_{102\times302} - f_{202\times602})}{\ln(r)}, \quad r = 2, \quad (15)$$

where $f_{m\times n}$ denotes the solution on the $m \times n$ grid and r is the grid refinement ratio that is constant and equals 2. Although very good grid convergence is found for the velocities, the convergence of $\psi_{\min}$ and $\|E_k\|_1$ shows behavior that is not entirely clear and prevents a rigorous characterization of the order of grid convergence. Despite that an estimate of accuracy of the solution on the finest grid, the grid convergence index (GCI):

$$\text{GCI}_{202\times602} = \frac{3}{r^p - 1}\left|\frac{f_{102\times302} - f_{202\times602}}{f_{202\times602}}\right|, \quad r = 2, \; p = 2, \quad (16)$$

was computed, assuming an order of convergence $p = 2$, which is the theoretical order of accuracy of the discretization methods. The results indicate that the solution is probably well-converged but that it is not straightforward to perform a clear and rigorous grid convergence characterization using Richardson-extrapolation based techniques. To investigate in more detail the flow problem and its numerical behavior the solution is studied on a further simplified case of thermal convection in a cavity that enables more rigorous verification and a comparison with a different numerical method.

6. Thermal natural convection in a rectangular cavity

The finite-volume DC casting code (FVM) is further tested on a problem of transient thermal natural convection in a rectangular cavity, which was devised to be prototypal for the flow during the initial stages of solidification in a cavity. The problem considers a liquid metal in a cavity with insulated top and bottom walls, of width L and height H, that is initially at the temperature of the left wall T_H. At time $t = 0$ a constant lower temperature T_C is imposed at the right wall. The asymmetric cooling induces a transient flow, which evolves into an unsteady multicellular structure. After the initial transient the system evolves into a periodic oscillatory flow. The system is characterized by $Pr = 0.0137$, $Ra = 2.81 \times 10^5$ (both parameters correspond to the thermophysical properties of Al-4.5%Cu (Vreeman and Incropera, 2000), a wall

Grid	$u_{\min}$ (m/s)	$v_{\min}$ (m/s)	$\psi_{\min}$ (m^3/s)	$\|E_k\|_1$(J)
27×77	-1.782×10^{-2}	-0.982×10^{-2}	-1.217×10^{-2}	3.425×10^{-4}
52×152	-2.151×10^{-2}	-1.116×10^{-2}	-1.129×10^{-5}	3.464×10^{-4}
102×302	-2.337×10^{-2}	-1.312×10^{-2}	-1.108×10^{-5}	3.482×10^{-4}
202×602	-2.363×10^{-2}	-1.355×10^{-2}	-1.116×10^{-5}	3.500×10^{-4}
p_{Rex}	2.8	2.2	–	-0.007
$\text{GCI}_{202\times602}(p = 2)$(percent)	1.1	3.2	0.7	0.5

Table I. Grid convergence of velocity and streamfunction minima and of the discretized L_1 norm of the kinetic energy for the thermal DC casting problem

temperature difference of 40 K and a cavity height of 0.05 m), and an aspect ratio $A = H/L = 4$. The results are presented in dimensionless form, with the variables scaled as:

$$X = \frac{x}{H}, \quad Y = \frac{y}{H}, \quad t^* = \frac{\kappa\sqrt{Ra_T}}{H^2}\, t, \quad (u^*, v^*) = \frac{H}{\kappa\sqrt{Ra_T}}(u, v),$$
$$\psi^* = \frac{1}{\kappa\sqrt{Ra_T}}\, \psi, \quad \theta = \frac{T - T_H}{T_H - T_C} \tag{17}$$

where H is the cavity height, κ is the thermal diffusivity, t is the time, and ψ is the streamfunction.

The results are compared to the solution obtained by the SCM (Xin and Le Quéré 2002), which are verified to be grid independent. Additionally, a grid convergence study of the FVM solution involving four grids is made. Such a combined verification approach gives a very high level of confidence. In the code comparison (Figures 3 and 4) the FVM solution obtained on a uniform 100 × 400 grid and using a dimensionless time step of $\Delta t^* = 8.91 \times 10^{-2}$ is presented. As already pointed out in Section 2.3, FVM discretization schemes were used that are theoretically at least second-order accurate in space and first-order accurate in time. The SCM solution was obtained on a Gauss-Lobatto spatial resolution of 59 × 101 and a dimensionless time step of

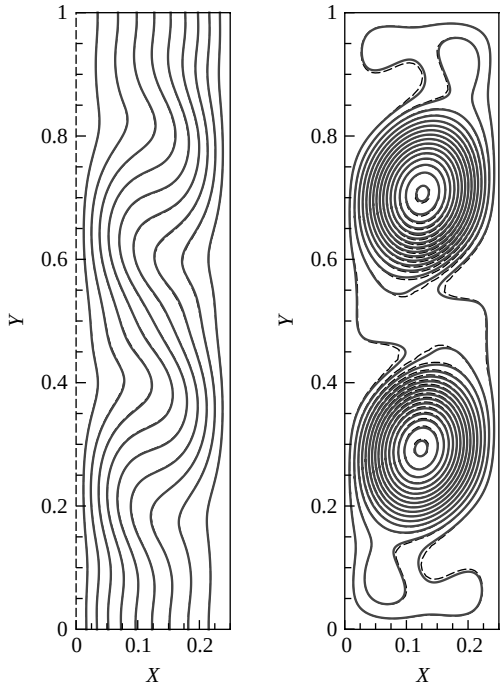

Notes: FVM (100 × 400)—solid line; SCM—dashed line

Figure 3.
Temperature and flow fields ($\Delta\theta = 0.1$; $\Delta\psi^* = 0.005$) in the cavity at same phase angle

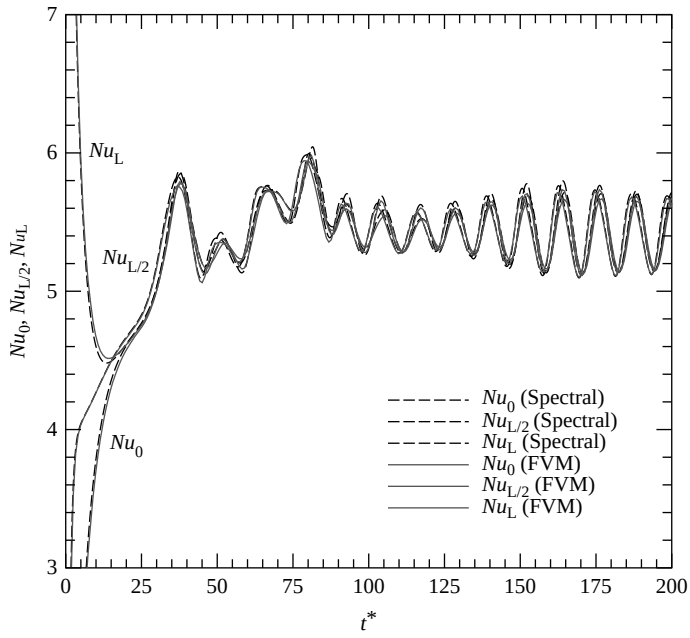

Note: Comparison of the FVM (100 × 400) and SCM

Figure 4.
Time evolution of the Nusselt number at the left (Nu_0) and right (Nu_L) walls and the midplane ($Nu_{L/2}$) of the cavity

$\Delta t^* = 10^{-2}$ using a second-order accurate timestepping scheme. The streamlines and temperature contours at the oscillation phase angle corresponding to the state obtained by the spectral method at $t^* = 1{,}000$ are shown in Figure 3. Note that the final period of the oscillations is the same in both computations, however there is a small phase shift. The time evolution of the Nusselt number at both walls and at the center plane is shown in Figure 4. Overall, the agreement of the FVM and SCM solutions is extraordinary, especially with regard to the challenging problem.

Aiming at a rigorous verification and with the objective of elucidating the convergence behavior of the FVM flow solution, which was somewhat unclear in the thermal DC casting problem, a grid convergence study over four grids (13 × 50, 25 × 100, 50 × 200, and 100 × 400) with discretization-error estimation is made. A detailed investigation of grid convergence of all quantities over the entire domain in the state shown in Figure 3 revealed that the convergence is oscillatory. Therefore, the approximate error spline (AES) method (Celik *et al.*, 2005) is used to compute an extrapolated solution. The error band GCI of the extrapolated solution is calculated according to (Roache, 1998):

$$\mathrm{GCI}_{\mathrm{AESex}} = \frac{1}{r^p - 1}\left|\frac{f_{100\times400} - f_{\mathrm{AESex}}}{f_{\mathrm{AESex}}}\right|, \quad r = 2,\ p = 2, \tag{18}$$

where AESex denotes the AES-extrapolated solution and the theoretical order of convergence $p = 2$ is used. The results of the grid convergence study summarized in Table II indicate a very good accuracy, showing that the error band of the extrapolated solution is well below 0.5 percent and the difference between the 100 × 400-grid and the

extrapolated solutions is within a margin of less than 1 percent. The excellent result of the FVM-SCM code comparison and the demonstrated grid convergence infer a very high level of confidence in both codes and affirm a successful step in the verification of the flow model of the DC casting code.

7. Coupled transport of heat, mass, and species in the mushy zone

The proper solution of the coupling of the continuity, energy, and species conservation equations, and the microsegregation model, which defines the solute partitioning of the solid and liquid phases in the mushy zone as well as the temperature and liquid fraction in the enthalpy formulation, is essential for the prediction of shrinkage-induced macrosegregation (Figure 1). As part of the full model this coupling is verified by comparison with Voller's (1997b) similarity solution for 1D directional solidification. The solidification of an Al-5%Cu alloy proceeds in an insulated vertical mold with a bottom ($z = 0$) cooled at a constant temperature below the solidus temperature of the alloy. Initially the liquid alloy has a uniform concentration at 5%Cu and a uniform temperature slightly above the liquidus. The mold is considered long enough such that the temperature and concentration at its top remain at the initial values throughout. During solidification three zones form – a solid zone at the bottom, a mushy zone between the eutectic and liquidus temperatures and a liquid zone at the top. A flow of enriched liquid towards the bottom is induced by solidification shrinkage in the mushy zone. The flow drives the advective transport towards the eutectic front and produces positive macrosegregation (inverse segregation) in the solidified bottom part and a solute-depleted mushy zone. The similarity solution is formulated using a similarity variable $\xi = z/\sqrt{\kappa t}$, such that it reduces the governing PDEs, equations (4), (7) and (8), to a set of ODEs. This set is solved analytically in the fully solid and liquid parts and with a Runge-Kutta method in the mushy part. The introduction of the similarity variable also transforms the transient problem (dependent on z and t) into a steady problem in terms of ξ. A comparison of the similarity solution and the numerical solution is shown in Figure 5. The transient numerical solution is obtained with the finite-volume macrosegregation code on a 4×402 grid and transformed into the ξ-space. It is shown for 15 different times, $t = 10, \ldots 150$ s, evenly distributed at $\Delta t = 10$ s. The considerable discrepancy in the concentration profile is attributed to a numerical problem related to the resolution of the exact position of the eutectic front. The problem was found to be identical to the problem known from fixed-grid numerical solutions of the Stefan problem (Voller, 1997a). Here, it effectively causes oscillations of the vertical velocity ($U^* = \sqrt{t/\kappa v}$), shown in the profile in Figure 5(a), which strongly deteriorates the solution of the predominantly advective solute transport.

Table II.
Grid convergence of velocity and streamfunction maxima of the FVM solution, and the approximate-error-spline extrapolated solution (AESex)

Grid	u^*_{max}	v^*_{max}	$\lvert\psi^*\rvert_{max}$
13×50	1.060	3.051×10^{-2}	3.93017×10^{-2}
25×100	1.019	2.940×10^{-2}	3.91031×10^{-2}
50×200	1.032	2.989×10^{-2}	3.99413×10^{-2}
100×400	1.038	3.023×10^{-2}	4.00588×10^{-2}
AESex	1.040	3.039×10^{-2}	4.00448×10^{-2}
$GCI_{\text{AESex (percent)}}$	0.1	0.3	0.005

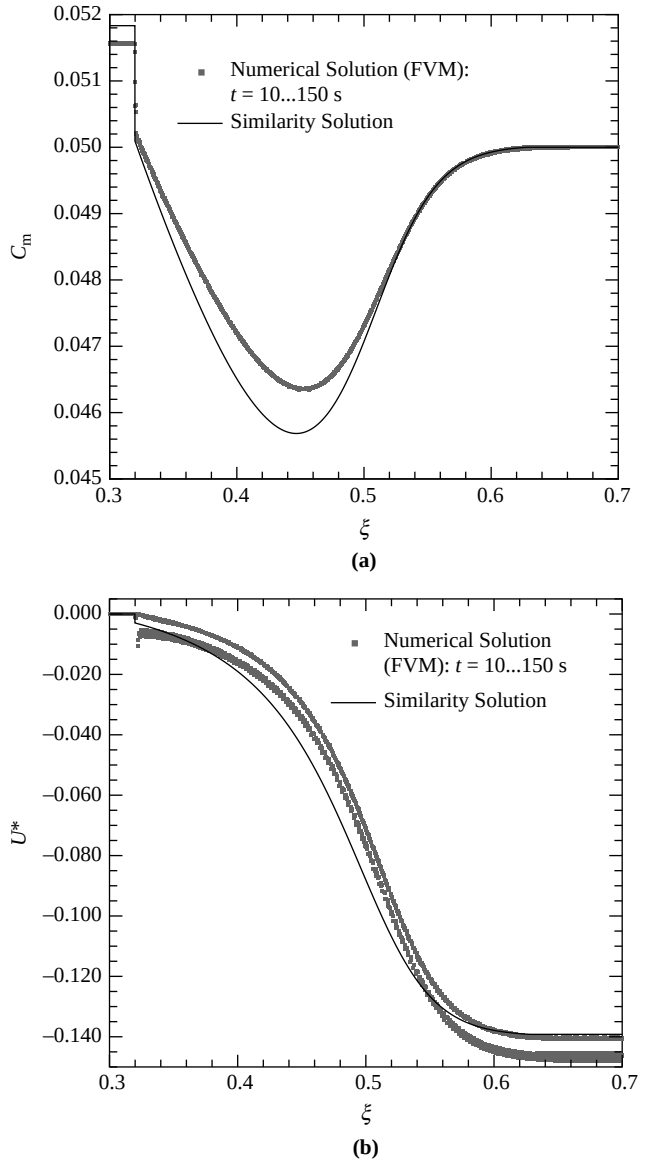

Notes: (a) Concentration profile; (b) Shrinkage induced velocity

Figure 5.
Comparison of the FVM numerical solution and the reference similarity solution presented in terms of the similarity variable $\xi = z/\sqrt{\kappa t}$

8. Conclusions

The verification of the finite-volume based code developed for the simulation of macrosegregation in DC casting has shown an excellent ability of the model to accurately resolve the thermal convection in the pertinent parameter range of Pr and Ra_T. With regard to this conclusion, the failure to rigorously characterize the grid

convergence of the thermal convection flow solution in the realistic DC casting geometry by Richardson extrapolation, shows that grid-convergence analysis of such problems is not straightforward and more sophisticated techniques, such as the approximate-error-spline method, may have to be used. Additionally, an optimization of numerical parameters, i.e. grid spacing, local grid refinement in the porous solidification region, could improve accuracy and speed up grid convergence. Concerns regarding the solution of species transport in the mushy zone remain, although it is not completely clear how the problems encountered in the solution of the transient reference solidification problem relate to the steady mushy zone in DC casting. Further verification steps of the DC casting code will consist of problems of thermosolutal natural convection in simple geometries.

References

Bennon, W.D. and Incropera, F.P. (1987), "A continuum model for momentum, heat and species transport in binary solid-liquid phase change systems – I. Model formulation", *International Journal of Heat and Mass Transfer*, Vol. 30 No. 10, pp. 2161-70.

Celik, I., Li, J., Hu, G. and Shaffer, O. (2005), "Limitations of Richardson extrapolation and some possible remedies", *Journal of Fluids Engineering ASME*, Vol. 127, pp. 795-805.

Ferziger, J.H. and Perić, M. (2002), *Computational Methods for Fluid Dynamics*, Springer-Verlag, Berlin.

Gobin, D. and Bennacer, R. (1996), "Cooperating thermosolutal convection in enclosures – II. Heat transfer and flow structure", *International Journal of Heat and Mass Transfer*, Vol. 39 No. 13, pp. 2683-97.

Jalanti, T., Swierkosz, M., Gremaud, M. and Rappaz, M. (2001), "Modelling of macrosegregation in continuous casting of aluminium", in Ehrke, K. and Schneider, W. (Eds), *Continuous Casting*, DGM, Weinheim, pp. 191-8.

Leonard, B.P. (1997), "Bounded higher-order upwind multidimensional finite-volume convection-diffusion algorithms", in Minkowycz, W.J. and Sparrow, E.M. (Eds), *Advances in Numerical Heat Transfer*, Taylor & Francis, Bristol, PA, pp. 1-57.

Perko, J. (2005), "Modelling of transport phenomena by the diffuse approximate method", PhD thesis, Nova Gorica Polytechnic, Nova Gorica, Slovenia.

Reddy, A.V. and Beckermann, C. (1997), "Modeling of macrosegregation due to thermosolutal convection and contraction-driven flow in direct chill continuous casting of an Al-Cu Round Ingot", *Metallurgical and Materials Transactions B*, Vol. 28B No. 3, pp. 479-89.

Roache, P.J. (1998), *Verification and Validation in Computational Science and Engineering*, Hermosa, Albuquerque, NM.

Roy, C.J. (2005), "Review of code and solution verification procedures for computational simulation", *Journal of Computational Physics*, Vol. 205 No. 1, pp. 131-56.

Saunders, N., Li, X., Miodownik, A.P. and Schillé, J-P. (2001), "Computer modeling of materials properties", in Zhao, J.-C *et al.* (Eds), *Materials Design Approaches and Experiences*, TMS, Warrendale, PA, pp. 185-97.

Venneker, B.C.H. and Katgerman, L. (2002), "Modelling issues in macrosegregation predictions in direct chill castings", *Journal of Light Metals*, Vol. 2 No. 3, pp. 149-59.

Voller, V.R. (1997a), "An overview of numerical methods for solving phase change problems", in Minkowycz, W.J. and Sparrow, E.M. (Eds), *Advances in Numerical Heat Transfer*, Taylor & Francis, Bristol, PA, pp. 341-80.

Voller, V.R. (1997b), "A similarity solution for the solidification of a multicomponent alloy", *International Journal of Heat and Mass Transfer*, Vol. 40 No. 12, pp. 2869-77.

Vreeman, C.J. and Incropera, F.P. (2000), "The effect of free-floating dendrites and convection on macrosegregation in direct chill cast aluminum alloys, part II: predictions for Al-Cu and Al-Mg alloys", *International Journal of Heat and Mass Transfer*, Vol. 43 No. 5, pp. 687-704.

Xin, S. and Le Quéré, P. (2002), "An extended chebyshev pseudo – spectral benchmark for the 8:1 differentially – heated cavity", *International Journal of Numerical Methods in Fluids*, Vol. 40 No. 8, pp. 981-98.

Založnik, M. (2006), *Modeling of Macrosegregation in Direct Chill Casting*, PhD thesis, University of Nova Gorica, Nova Gorica.

Založnik, M. and Šarler, B. (2005a), "Modeling of macrosegregation in DC casting of aluminum alloys: estimating the influence of casting parameters", *Materials Science & Engineering A*, Vol. 413/414, pp. 85-91.

Založnik, M. and Šarler, B. (2005b), "New insights into flow structure in the DC casting of aluminum alloys", in Kvande, H. (Ed.), *Light Metals 2005*, TMS, Warrendale, PA, pp. 1031-6.

Appendix

Solid density	ρ_s (kg/m^3)	2750[a]
Liquid density	ρ_l (kg/m^3)	2460[a]
Solid specific heat	c_{ps} (J/kgK)	1030[a]
Liquid specific heat	c_{pl} (J/kgK)	1130[a]
Solid thermal conductivity	k_s (W/mK)	180[a]
Liquid thermal conductivity	K_l (W/mK)	80[a]
Solid diffusivity	D_s (m^2/s)	5×10^{-12} [b]
Liquid diffusivity	D_l (m^2/s)	5×10^{-9} [a]
Latent heat at eutectic	L_{eut} (J/kg)	3.77×10^{5} [a]
Liquid viscosity	μ (Pas)	1.3×10^{-3} [a]
Thermal expansion coefficient	β_T (K^{-1})	1.17×10^{-4} [b]
Solutal expansion coefficient	$\beta_{C\ (-)}$	-0.73[b]
Reference temperature	T_0 (K)	973.15
Reference concentration	C_0 (–)	0.0525
Reference density	ρ_0 (kg/m^3)	2460
Permeability constant	K_0 (m^2)	6.67×10^{-11} [b]
Pure Al melting temperature	T_f (K)	933.6[a]
Al-Cu eutectic temperature	T_{eut} (K)	821.2[a]
Eutectic solidification interval	ΔT_{eut} (K)	1
Liquidus slope	m_l (K)	338.45
Partition coefficient	k_p (–)	0.173

Source: [a]JMatPro software (Saunders *et al.*, 2001); [b]Vreeman and Incropera (2000)

Table AI. Thermophysical properties of Al-5.25 wt%Cu

See Table AII on following page.

Corresponding author
Miha Založnik can be contacted at: miha.zaloznik@mines.inpl-nancy.fr

Table AII.
Process parameters and boundary conditions for the DC casting cases

Billet diameter	d (m)	0.282
Mold inlet diameter	d_{in} (m)	0.172
Cu concentration at inlet	C_{cast} (–)	0.0525
Melt temperature at inlet	T_{cast} (K)	973.15
Casting velocity	v_{cast} (m/s)	1.25
Inlet velocity	$v_{in} = (\rho_s/\rho_l)(d/d_{\text{in}})^2 v_{\text{cast}}$	
Cooling heat transfer coefficient:		
$h_{\text{chill}} = \begin{cases} 0[W/m^2K]z > -0.03\,\text{m} 5000^{f_l} \cdot 400^{(1-f_l)}[W/m^2K] - 0.03\,\text{m} > z > -0.04\,\text{m} \\ [-1.67 \cdot 10^5 + 352(T + T_w)[K]] \cdot (Q_w[m^3/s]/\pi D[m])^{1/3} - 0.04\,\text{m} > z \\ +20.8(T[K] - T_{\text{sat}}[K])^3[W/m^2K] \\ \text{Coolingwaterentrytemperature} \end{cases}$	T_{w} (K)	300
Cooling water flow rate	Q_{w} (m^3/s)	1.75×10^{-3}